Transactions of JASCOME, Journal of Boundary Element Methods, Vol. 20 (Dec. 2003), No. 06-030928 JASCOME

BOUNDARY-TYPE MESHLESS SOLUTIONS OF POTENTIAL PROBLEMS: COMPARISON BETWEEN SINGULAR AND REGULAR FORMULATIONS IN HYBRID BNM

Masataka TANAKA [1], Jianming ZHANG [2], Toshiro MATSUMOTO [3]

1) Faculty of Engineering, Shinshu University, (Nagano 380-8553, e-mail: dtanaka@gipwc.shinshu-u.ac.jp)

2) Faculty of Engineering, Shinshu University, (Nagano 380-8553, e-mail: zhangjm@homer.shinshu-u.ac.jp)

3) Faculty of Engineering, Shinshu University, (Nagano 380-8553, e-mail: toshiro@gipwc.shinshu-u.ac.jp)

We have recently presented two types of the hybrid boundary node methods, the singular hybrid boundary node method (SHBNM) and the regular hybrid boundary node method (RHBNM). Both the methods combine a modified functional with the moving least squares (MLS) approximation, and are truly meshless, boundary-only methods. SHBNM and RHBNM formulations are developed for solving 3-D potential problems. Numerical examples are computed and the results obtained are discussed. Emphasis is placed on studying parameters which influence the performances of them. Their convergence rates and applicability to thin structures are investigated.

Keywords: meshless methods; hybrid boundary node method; moving least squares approximation

1. Introduction

One of the most time-consuming parts of numerical analyses by domain-type methods is the discretization of domain of interest. If the domain is of complex geometry, the task of an implementation of FEM is usually challenging. The BEM-based models partially alleviate the problem as the discretization of only boundary surface is required. However, still in many cases it may be difficult and cumbersome to prepare the necessary input data for elements. Combining the BEM with the meshless techniques may be an attractive way for avoiding the mesh generation requirements. Recently, several meshless methods for boundary-only analysis have been proposed in the literature. One possibility in this approach is the boundary node method (BNM) [1].

The BNM is a combined boundary integral/meshless approach for boundary only analysis of partial differential equations. In the BNM, given a scattered set of points, meshless interpolation functions are constructed by using a moving least-squares approach [2], so that no boundary mesh is needed for interpolation of variables. However, for boundary integration, they have to construct a background boundary cells structure.

In order not to create the background cells and hence achieve a truly meshless method, we have developed two meshless methods: the singular hybrid boundary node method (SHBNM) [3] and the regular hybrid boundary node method (RHBNM) [4]. Both the methods use local weak forms over a local sub-domain and shape functions from the MLS approximation, and are truly meshless, as no 'boundary element mesh' is generated either for the variable interpolation or for the boundary integration. All integrals can be easily evaluated over regularly shaped local boundary regions.

The SHBNM was first proposed. However, the SHBNM has a drawback of serious "boundary layer effect", i.e. the accuracy of results in the vicinity of the boundary is very sensitive to the proximity of the interior points to the boundary. To avoid this drawback, we then proposed the RHBNM. In contrast to SHBNM and other hybrid boundary element models [5], the fundamental solutions are used in the RHBNM with their source points located outside the domain rather than on the boundary. Numerical computations show that results from the RHBNM are not sensitive to the proximity of the interior points to the boundary and very high accuracy can be achieved even when a small number of boundary nodes are used. However, the outside arrangement of the source points of the fundamental solution also has some disadvantages. The advantages and disadvantages of these two meshless methods have not been discussed in detail in the published papers. So far, their applications were very limited. Hence, further research work about SHBNM and RHBNM are necessary.

In this paper, SHBNM and RHBNM are examined and compared in detail. Their formulations and implementations are first presented for 3-D potential problems. Then, parameters that influence the performance of them are studied through numerical examples.

2. Local weak form for a hybrid model

The potential problem in three dimensions governed by Laplace's equation with boundary conditions is written as

$$\begin{aligned} u_{,ii} &= 0, \quad \forall x \in \Omega \\ u &= \bar{u}, \quad \forall x \in \Gamma_u \\ u_{,i} n_i &\equiv q = \bar{q}, \quad \forall x \in \Gamma_q \end{aligned} \tag{1}$$

where the domain Ω is enclosed by $\Gamma = \Gamma_u + \Gamma_q$; $\bar{u}$ and $\bar{q}$ are the prescribed potential and the normal flux, respectively,

on the boundary parts Γ_u and Γ_q; and n is the outward normal direction to the boundary Γ, with components n_i, i =1,2,3.

The hybrid boundary node method proposed in this paper is based on a modified variational principle. The functions assumed to be independent are:

– potential field in the domain, u;

– boundary potential field, $\tilde{u}$;

– boundary normal flux, $\tilde{q}$.

The corresponding variational functional Π_{AB} is defined as follows:

$$\Pi_{AB} = \int_\Omega \frac{1}{2} u_{,i} u_{,i} d\Omega - \int_\Gamma \tilde{q}(u-\tilde{u}) d\Gamma - \int_{\Gamma_q} \overline{q}\tilde{u} d\Gamma \quad (2)$$

where, the boundary potential $\tilde{u}$ satisfies the essential boundary condition, i.e., $\tilde{u} = \overline{u}$ on Γ_u.

The variation of Π_{AB} becomes

$$\begin{aligned} \delta\Pi_{AB} = & \int_\Gamma (q-\tilde{q})\delta u d\Gamma - \int_\Omega u_{,ii}\delta u d\Omega \\ & + \int_{\Gamma_q} (\tilde{q}-\overline{q})\delta\tilde{u} d\Gamma - \int_\Gamma (u-\tilde{u})\delta\tilde{q} d\Gamma \end{aligned} \quad (3)$$

The vanishing of $\delta\Pi_{AB}$ for arbitrary variations δu in Ω, $\delta\tilde{u}$ and $\delta\tilde{q}$ on Γ, with $\delta\tilde{u} = 0$ on Γ_u, gives the following Euler equations:

$$\begin{aligned} u_{,ii} &= 0, \quad in \quad \Omega \\ u-\tilde{u} &= 0, \quad on \quad \Gamma \\ q-\tilde{q} &= 0, \quad on \quad \Gamma \\ \tilde{q}-\overline{q} &= 0, \quad on \quad \Gamma_q \end{aligned} \quad (4)$$

Consequently the solution of the problem is now given in terms of the functions u, $\tilde{u}$ and $\tilde{q}$, which makes $\delta\Pi_{AB}$ stationary.

With the vanishing of $\delta\Pi_{AB}$, we also have the following equivalent integral equations:

$$\int_\Gamma (q-\tilde{q})\delta u d\Gamma - \int_\Omega u_{,ii}\delta u d\Omega = 0 \quad (5)$$

$$\int_\Gamma (u-\tilde{u})\delta\tilde{q} d\Gamma = 0 \quad (6)$$

$$\int_{\Gamma_q} (\tilde{q}-\overline{q})\delta\tilde{u} d\Gamma = 0 \quad (7)$$

If we impose the flux boundary condition, $\tilde{q} = \overline{q}$, just in the same way as the essential boundary condition after the matrices have been computed, the Eq. (7) holds. So it can be omitted temporarily in the following development.

Equations (5) and (6) hold for any sub-domain Ω_s and its boundary $\partial\Omega$. $\partial\Omega$ consists of two parts, Γ_s and L_s (see Figure 1), where Γ_s is a portion of Γ; L_s is inside Ω. Following the procedure in Reference [6], we use the following weak forms for a sub-domain Ω_s and its boundary Γ_s and L_s to replace Eqs. (5) and (6):

$$\int_{\Gamma_s+L_s} (q-\tilde{q})v d\Gamma - \int_{\Omega_s} u_{,ii} v d\Omega = 0 \quad (8)$$

$$\int_{\Gamma_s+L_s} (u-\tilde{u})v d\Gamma = 0 \quad (9)$$

where v is a test function. It should be noted further that the above equations hold irrespective of the size and the shape of Ω_s and its boundary $\partial\Omega_s$. This is an important observation which forms the basis of the present formulation.

We now deliberately choose a simple regular shape for Ω_s. The most regular shape for a sub-domain in 3D space is sphere. In the present paper, we choose Ω_s as the intersection of the domain Ω and a sphere centered at a boundary node $\mathbf{s}_J$ (see Figure 1).

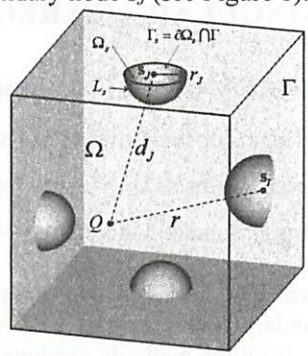

Figure 1. The local domain centered at a node $\mathbf{s}_J$ and the source point corresponding to a node $\mathbf{s}_I$.

In Eqs. (8) and (9), $\tilde{u}$ and $\tilde{q}$ on Γ_s are expressed by

$$\tilde{u}(\mathbf{s}) = \sum_{I=1}^{N} \Phi_I(\mathbf{s})\hat{u}_I \ , \ \tilde{q}(\mathbf{s}) = \sum_{I=1}^{N} \Phi_I(\mathbf{s})\hat{q}_I \quad (10)$$

where $\Phi_I(\mathbf{s})$ is the shape function of the MLS (see [4]), for Γ_s is a part of the globe boundary. However, $\tilde{u}$ and $\tilde{q}$ on L_s has not been defined yet. To solve this problem, we select v such that all integrals over L_s vanish. This can be easily accomplished by using the weight function in the MLS approximation for v, with the half-length of the major axis $\hat{d}_I$ of the support of the weight function being replaced by the radius r_J of the sub-domain Ω_s, i.e.

$$v_J(Q) = \begin{cases} \dfrac{\exp[-(d_J/c_J)^2] - \exp[-(r_J/c_J)^2]}{1-\exp[-(r_J/c_J)^2]}, & 0 \le d_J \le r_J \\ 0, & d_J \ge r_J \end{cases} \quad (11)$$

where d_J is the distance between a point Q, in the domain Ω, and the nodal point $\mathbf{s}_J$. Therefore, v vanishes on L_s. Thus we obtain the local weak form as follows:

$$\int_{\Gamma_s} (q-\tilde{q})v d\Gamma - \int_{\Omega_s} u_{,ii} v d\Omega = 0 \quad (12)$$

$$\int_{\Gamma_s} (u-\tilde{u})v d\Gamma = 0 \quad (13)$$

with the boundary integrations all restricted on the sub-region Γ_s.

2.1 Numerical implementation for SHBNM

In Eqs. (12) and (13), we approximate u in the domain with

$$u = \sum_{I=1}^{NN} U_I x_I \quad (14)$$

and hence

$$q = \sum_{I=1}^{NN} \frac{\partial U_I}{\partial n} x_I \quad (15)$$

where U_I is the fundamental solution; x_I are weight parameters; NN is the total number of boundary nodes.

For 3-D potential problem, the fundamental solution is

$$U_I = \frac{1}{4\pi} \frac{1}{r(Q, P_I)} \quad (16)$$

where Q and P_I are the field point and the source point respectively. And P_I is located on the boundary and coincident with the node point $\mathbf{s}_I$.

As u is expressed by Eq. (14), the last integral on the left-hand side in Eq. (12) vanishes if one excludes node s_J at which singularity occurs from the sub-domain Ω_s. This singularity will be considered when evaluating the boundary integrals.

By substituting Eqs. (10), (11), (14) and (15) into Eqs. (12) and (13), and supposing that all nodes are on smooth portions of Γ, we have

$$\frac{1}{2}x_J + \sum_{I=1}^{n}\int_{\Gamma_s}\frac{\partial U_I}{\partial n}v_J(Q)x_I d\Gamma = \sum_{I=1}^{n}\int_{\Gamma_s}\Phi_I(s)v_J(Q)\hat{q}_I d\Gamma$$

$$\sum_{I=1}^{n}\int_{\Gamma_s}U_I v_J(Q)x_I d\Gamma = \sum_{I=1}^{n}\int_{\Gamma_s}\Phi_I(s)v_J(Q)\hat{u}_I d\Gamma \tag{17}$$

In the present formulation, the proper choice of the integration boundary Γ_s is particularly important for 3-D problems. The theoretically ideal Γ_s is chosen in such a way that they cover the whole boundary of the body and does not overlap each other. Unfortunately, this condition can not be realized in 3-D case. However, from our computation in 2-D case, the present formulation is expected to give acceptable results in cases when the local regions Γ_s, each of them containing one node only, overlap each other, or the union of all local regions Γ_s does not cover the whole boundary[3,7]. Therefore, in this paper, we use ellipse in the parametric plane for the shape of the local regions Γ_s and investigate the optimal size of Γ_s.

Using the above equations for all nodes, we obtain the following system of equations

$$\mathbf{U}\mathbf{x} = \mathbf{H}\hat{\mathbf{q}} \tag{18}$$

$$\mathbf{V}\mathbf{x} = \mathbf{H}\hat{\mathbf{u}} \tag{19}$$

where

$$U_{IJ} = \int_{\Gamma_s^J}\frac{\partial U_I}{\partial n}v_J(Q)d\Gamma$$

$$V_{IJ} = \int_{\Gamma_s^J}U_I v_J(Q)d\Gamma$$

$$H_{IJ} = \int_{\Gamma_s^J}\Phi_I(s)v_J(Q)d\Gamma$$

$$\mathbf{x}^T = [x_1, x_2, \cdots, x_n]$$

$$\hat{\mathbf{q}}^T = [\hat{q}_1, \hat{q}_2, \cdots, \hat{q}_n]$$

$$\hat{\mathbf{u}}^T = [\hat{u}_1, \hat{u}_2, \cdots, \hat{u}_n]$$

and Γ_s^J is the local region Γ_s corresponding to the node s_J.

From Eq. (19) we have

$$\mathbf{x} = \mathbf{V}^{-1}\mathbf{H}\hat{\mathbf{u}} \tag{20}$$

Substituting Eq. (20) into (18), we have

$$\mathbf{U}\mathbf{V}^{-1}\mathbf{H}\hat{\mathbf{u}} - \mathbf{H}\hat{\mathbf{q}} = 0 \tag{21}$$

The evaluation of the matrix $\mathbf{U}$ is the most critical step in this approach, as integrations of singular functions are required. Accurate and appropriate numerical integration schemes have to be used for different types of singularities of the integrands. Since the main diagonal terms of matrix $\mathbf{U}$ can be calculated by applying a special solution (e.g. a constant field), however, the direct numerical evaluation of hyper-singular integrals can be avoided.

For a well-posed problem, either $\tilde{u}$ or $\tilde{q}$ is known at each node on the boundary. However, transformations between $\hat{u}_I$ and $\tilde{u}_I$, $\hat{q}_I$ and $\tilde{q}_I$ are necessary because the MLS interpolants lack the delta function property of the usual BEM shape functions. For the panels with specified potential boundary conditions, $\hat{u}_I$ is related to $\bar{u}_I$ by

$$\hat{u}_I = \sum_{J=1}^{N}R_{IJ}\tilde{u}_J = \sum_{J=1}^{N}R_{IJ}\bar{u}_J \tag{22}$$

and for the panels with specified normal flux boundary conditions, $\hat{q}_I$ is related to $\bar{q}_I$ by

$$\hat{q}_I = \sum_{J=1}^{N}R_{IJ}\tilde{q}_J = \sum_{J=1}^{N}R_{IJ}\bar{q}_J \tag{23}$$

where $R_{IJ} = \left[\Phi_J(s^I)\right]^{-1}$ (see Reference [6]).

Equation (21) can be solved in the same way as that in the conventional BEM. Then, the unknown vector $\mathbf{x}$ is obtained by Eq. (20). As can be seen, the present method is a truly meshless one. No boundary elements are used for interpolation nor integration purposes.

2.2 Numerical implementation for RHBNM

The numerical implementation for RHBNM is almost the same as that for SHBNM, except that, to avoid singularities, the source point P_I of the fundamental solution is located outside the domain and determined by

$$P_I = \mathbf{s}_I + \mathbf{n}(\mathbf{s}_I)\cdot h\cdot SF \tag{24}$$

where h is the nearest distance between the neighbouring nodes; $\mathbf{n}(\mathbf{s}_I)$ is the unit outward normal to the boundary at node s_I; and SF is a scale factor. The scale factor, SF, plays an important role in the performance of the RHBNM method. Too small value for SF will lead to nearly singular integrals and thus inaccurate results; On the other hand, too large one will lead to an ill-conditioned system of algebraic equations. The optimal value of SF will be suggested by numerical computations.

As the source point P_I of the fundamental solution is located outside the domain, the last integral at the left hand in Eq. (12) vanishes without excluding the node s_J from the sub-domain Ω_s. Therefore, there is no singularity in the matrices $\mathbf{U}$ and $\mathbf{V}$ at all. By rearranging Eqs. (18) and (19), we can have the following final equation to determine the unknown vector $\mathbf{x}$.

$$\mathbf{A}\mathbf{x} = \mathbf{d} \tag{25}$$

where $\mathbf{A}$ and $\mathbf{d}$ are formed by merging $\mathbf{U}$ and $\mathbf{V}$, $\mathbf{H}\hat{\mathbf{u}}$ and $\mathbf{H}\hat{\mathbf{q}}$ according the known boundary conditions. For degrees of freedom with specified potential boundary conditions, $\mathbf{H}\hat{\mathbf{u}}$ is selected for $\mathbf{d}$, and its corresponding row of $\mathbf{V}$ is selected for $\mathbf{A}$; otherwise, $\mathbf{H}\hat{\mathbf{q}}$ is selected for $\mathbf{d}$, and its corresponding row of $\mathbf{U}$ is selected for $\mathbf{A}$.

The evaluation of the matrices $\mathbf{U}$ and $\mathbf{V}$ is much simpler in RHBNM than SHBNM because it is singularity-free. Furthermore, the inverse of $\mathbf{V}$ is also avoided.

3. Secondary results recovery

The secondary results recovery processes in SHBNM and RHBNM are considerably different. In RHBNM, the secondary results can be computed easily. After $\mathbf{x}$ being obtained by solving Eq. (25), potential u and flux q at any point inside domain Ω or on boundary Γ can be evaluated merely by Eqs. (14) and (15) without further integrations. Since u and q on boundary Γ can be evaluated in the same

way as that inside domain, the unknowns $\hat{\mathbf{q}}$ and $\hat{\mathbf{u}}$ need not to be obtained. However, in SHBNM, we cannot use Eqs. (14) and (15) to calculate u and q on the boundary, due to the singularities at the boundary. And if we evaluate u and q inside the domain using Eqs. (14) and (15), the serious "boundary layer effect" appears [3], since a near singularity occurs when the evaluation point is very near to a source point. The results recovery on the boundary and inside the domain must be performed in different ways. To circumvent the "boundary layer effect" in the SHBNM, an adaptive face integration scheme has been developed here for 3-D potential problems.

3.1. Potentials and potential gradients on the boundary in SHBNM

After solving Eq. (21), the unknowns $\hat{\mathbf{q}}$ and $\hat{\mathbf{u}}$ are ready for use to calculate the potential $\tilde{u}$ and normal flux $\tilde{q}$ on the boundary by using Eq. (10), respectively. For evaluating the potential gradients on the boundary, we use the following equation:

$$\begin{Bmatrix} \tilde{q} \\ \partial\tilde{u}/\partial s_1 \\ \partial\tilde{u}/\partial s_2 \end{Bmatrix} = \begin{bmatrix} n_1 & n_2 & n_3 \\ \partial x_1/\partial s_1 & \partial x_2/\partial s_1 & \partial x_3/\partial s_1 \\ \partial x_1/\partial s_2 & \partial x_2/\partial s_2 & \partial x_3/\partial s_2 \end{bmatrix} \begin{Bmatrix} q_1 \\ q_2 \\ q_3 \end{Bmatrix} \tag{26}$$

where q_i are potential gradients; $\partial x_i/\partial s_k$, k=1,2 are the tangent vectors of the boundary surface; and $\partial\tilde{u}/\partial s_k$ are calculated by

$$\partial\tilde{u}/\partial s_k = \sum_{I=1}^{N} \Phi_{I,k}\hat{u}_I \tag{27}$$

in which $\Phi_{I,k}$ are derivatives of MLS shape function.

3.2. Potentials and potential gradients at internal points in SHBNM

The potential u and the flux q at an internal point, P, are evaluated by the traditional boundary integral equations as follows:

$$u(P) = \int_\Gamma U(Q,P)\tilde{q}(Q)d\Gamma - \int_\Gamma \frac{\partial U(Q,P)}{\partial n(Q)}\tilde{u}(Q)d\Gamma \tag{28}$$

$$= \sum_{panels}\int_{\Gamma^p} U(Q,P)\tilde{q}(Q)d\Gamma - \sum_{panels}\int_{\Gamma^p}\frac{\partial U(Q,P)}{\partial n(Q)}\tilde{u}(Q)d\Gamma$$

$$q_i(P) = \int_\Gamma U(Q,P)\tilde{q}(Q)d\Gamma - \int_\Gamma \frac{\partial U(Q,P)}{\partial n(Q)}\tilde{u}(Q)d\Gamma \tag{29}$$

$$= \sum_{panels}\int_{\Gamma^p}\frac{\partial U(Q,P)}{\partial x_i(P)}\tilde{q}(Q)d\Gamma - \sum_{panels}\int_{\Gamma^p}\frac{\partial^2 U(Q,P)}{\partial x_i(P)\partial n(Q)}\tilde{u}(Q)d\Gamma$$

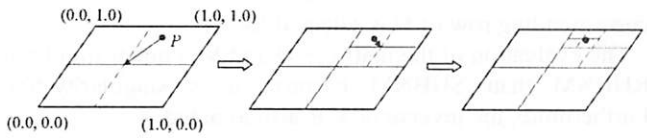

Figure 2 Subdividing of a panel in parametric space.

where $U(Q, P)$ is the fundamental solution with Q and P being the field point and source point, respectively. '*panels*' denotes the number of the panels which compose the whole boundary. Since every panel is represented by a unit square in parametric space, the integrals on each panel in Eqs. (28) and (29) can be easily computed. Here we develop an adaptive scheme to compute these integrals on a panel. In this scheme, the integrations are performed in the parametric unit square. We first divide the unit square into four equal quarters, (see Figure 2), then for each quarter, we calculate the diagonal length, l, and the distance between the evaluation point and the center of the quarter, d, in the global coordinate system. If l is smaller than d, this quarter is taken as a regular integration patch, or it is further divided into four sub-quarters, and the procedure goes on, until all patches become regular. Finally, using Gaussian quadrature for all patches, we can evaluate the integrals in Eqs. (28) and (29) very accurately even when the evaluation point is very close to the boundary. It should be pointed out that the patches are not like the standard elements in the BEM and FEM. They vary for different evaluation points and can be easily constructed. This does not change the fact that the hybrid boundary node method is a truly meshless method.

4. Numerical results

A quarter part of a hollow circular cylinder is modeled in Figure 3. The inner and outer radii of the hollow cylinder are R_1 = 10 and R_2 = 30, respectively. And the length L =10. The Laplace equation $\nabla^2 u = 0$ is solved here. Dirichlet boundary conditions are imposed at the cylindrical surfaces and Neumann boundary conditions at the other surfaces, corresponding to the following exact solutions:

$$u = x^3 + y^3 + z^3 - 3yx^2 - 3xz^2 - 3zy^2 \tag{30}$$

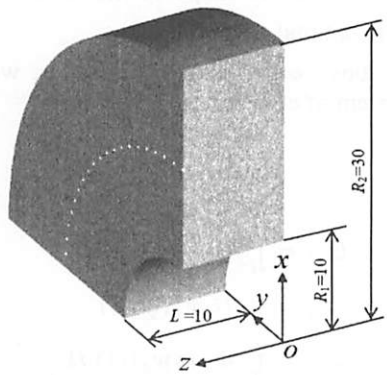

Figure 3 Dimensions of the hollow cylinder.

For the purpose of error estimation and convergence studies, a 'global' l_2 norm error, normalized by $|u|_{\max}$ is defined as

$$e = \frac{1}{|u|_{\max}}\sqrt{\frac{1}{N}\sum_{i=1}^{N}\left(u_i^{(e)} - u_i^{(n)}\right)^2} \tag{31}$$

where $|u|_{\max}$ is the maximum value of u over N sample points, the superscripts (e) and (n) refer to the exact and numerical solutions, respectively. Here we provide two error indicators, one for the variables inside the domain and the other for the variables on the boundary. The relative errors of u and its x-derivative inside the domain, denoted by DM-u and DM-q in the figures, are evaluated over 15 sample points uniformly distributed from (7.1, 7.1, 5.0) to (21,21,5.0) using Eq. (31); and the relative errors of u and q on the surface, denoted by SF-u and SF-q in the figures, are evaluated over 21 sample points uniformly spaced along a arc (with R=20) on the left face (shown as dots in Figure 3).

In the following two sections, we use this example for parameter and convergence studies. In all cases, unless

indicated otherwise, the size of the local domain (radius r_J) for each node is chosen as $0.75h$ in singular computations and $1.5h$ in regular computations. The parameter c_I in Eq. (11) is taken to be such that r_J/c_J is constant and equal to 1.0. The scale factor SF in Eq. (24) is assumed to be 3.0. To carry out the integration in Eq. (17), each of these local surfaces, Γ_s are mapped into a unit circle in the parametric space. The unit circle is divided into 8 parts, 2 segments in radial direction and 4 in circumferential direction. In each part, 5×5 Gauss points are used.

4.1 Parameter study

In this subsection, we study the optimal values of free parameters in SHBNM and RHBNM. There are many free parameters in the formulations of meshless methods, for example, the sub-domain radius r_J in RHBNM, SHBNM and the meshless local Petrov-Galerkin (MLPG) method [6]. The optimal values of these parameters were not theoretically determined, but suggested by empirical computations in the literature. So investigating how these parameters influence the performance of a meshless method is of critical importance. The sub-domain radius in SHBNM and RHBNM is firstly studied here. In the study, 1974 uniformly distributed boundary nodes are used in SHBNM computations, and 504 nodes in RHBNM computations. Computations are performed for various sub-domain radii, r_J. Relative errors for various sub-domain radii for SHBNM are presented in Figure 4 and for RHBNM in Figure 5. Note that the $\bigcup\Gamma_s$ do not cover the whole bounding surface when $r_J \le 0.5h$ (where h is the nearest distance between the neighbouring nodes), and the Γ_s will be overlapped when $r_J \ge 0.7h$. Figure 4 shows that results from SHBNM are in all case accurate no matter whether Γ_s are overlapped, or even uncover the body's boundary. The optimal value for r_J is between 0.75 h and 0.85 h. It is worth noting that r_J should be smaller than h in SHBNM, so that each sub-domain includes one node only, while in RHBNM there is no such limitation. This is because there is no singularity in RHBNM. Figure 5 demonstrates that the optimal value for r_J in RHBNM falls within the range from $1.5h$ to $2h$.

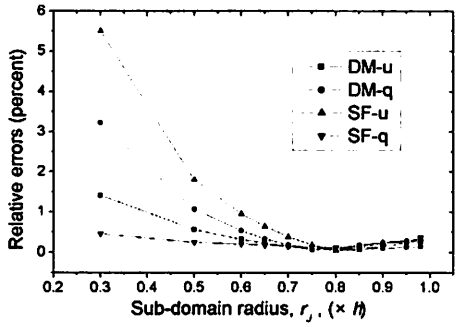

Figure 4. Relative errors for various sub-domain radius, r_J: singular formulations.

The scale factor SF in Eq. (24), plays a key role in the successful implementation of RHBNM. The relative errors for various SF in RHBNM computations are presented in Figure 6. It is seen that the relative errors as functions of SF are not stable, although results are accurate when $SF \ge 2.0$. The optimal value of SF is 7.0. As mentioned before, a large value of SF may lead to ill-conditioned equations and hence unstable results. Further computations show that the optimal value is independent of boundary condition, while strongly dependent on the domain geometry and nodes distribution. This parameter-dependence is a main drawback of RHBNM. To guarantee the stability, therefore, in this paper, we do not use the optimal value of SF, but instead SF=3.0. This value is chosen under a criterion that the SF should be as small as possible in case it gives acceptable results.

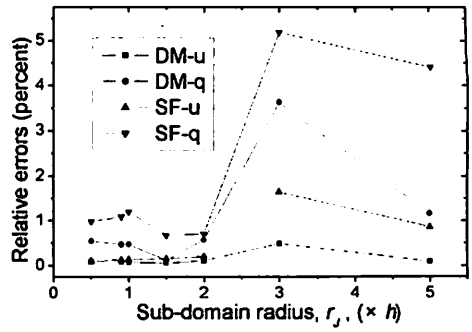

Figure 5. Relative errors for various sub-domain radius, r_J: regular formulations (SF=3.0).

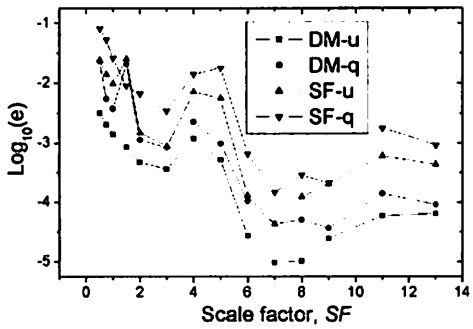

Figure 6. Relative errors for various scale factor, SF.

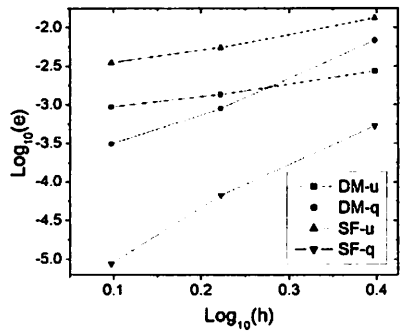

Figure 7. Convergence rates: singular formulations.

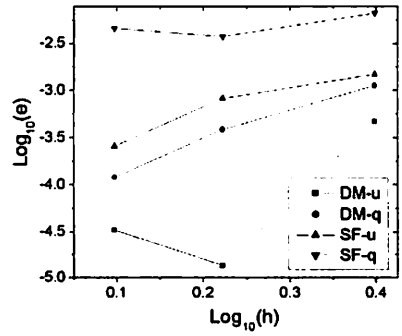

Figure 8. Convergence rates: regular formulations.

4.2 Convergence study

To study the convergence of the SHBNM and RHBNM,

the same problem in previous section is solved using three nodes arrangements: (a) 504 nodes, (b) 1118 nodes and (c) 1974 nodes uniformly distributed on the whole boundary. In RHBNM computations, a value of 3.0 is chosen for the scale factor *SF*. The relative errors for each nodes arrangement in SHBNM and RHBNM computations are presented in Figure 7 and Figure 8, respectively. In Figure 7 and Figure 8, h is the average distance between the neighbouring nodes. From Figure 7 and Figure 8, it is found that SHBNM processes much better convergence rate than RHBNM. The RHBNM can achieve high accuracy, but it is not very stable.

4.3 Applicability to thin structures

Thin structures are commonly used in engineering. The applicability of the RHBNM to thin structures has been verified by 2-D elasticity problems [8]. It was found that the RHBNM could be readily applied to thin structures with high accuracy. Here we verify the applicability of RHBNM and SHBNM to 3-D potential analysis of thin structures.

A cube with a spherical cavity centered is considered. The cube is of side length L =10. The Laplace equation $\nabla^2 u = 0$ is again considered here. Dirichlet and Neumann boundary conditions are imposed on the surfaces of the sphere and the cube, respectively, corresponding to Eq. (30). 20×20 nodes are uniformly spaced on each of the six faces of the cube, and 538 nodes on the surface of the sphere. The relative errors of potential and flux are evaluated over 21 sample points uniformly spaced at a straight segment from (1.15, 1.15, 1.15) to (5, 5, 5) using Eq. (31).

In this verification, we hold the dimensions of the cube constant while let the radius of cavity sphere vary in the range of $4.0 \le R \le 4.9999$. When the radius of the sphere approaches 5.0, the thickness at the centers of the six faces of the cube becomes nearly zero. This setup, therefore, provides a model which can be categorized as a non-uniform thin shell, a thick shell and even a bulky solid, according to the values of R. SHBNM and RHBNM computations have been performed for various values of R. In RHBNM computations, SF is taken to be 3.0. The relative errors for different R in SHBNM and RHBNM computations are presented in Table 1 and 2, respectively.

Table 1. Relative errors for different values of R in SHBNM.

R	4.8	4.9	4.99	4.999	4.9999
Error-u (%)	0.0524	0.259	1.108	23.43	fail
Error-q (%)	0.714	1.185	7.346	141.8	fail

Table 2. Relative errors for different values of R in RHBNM.

R	4.8	4.9	4.99	4.999	4.9999
Error-u (%)	0.01010	0.00885	0.00806	0.00800	0.00800
Error-q (%)	0.04259	0.04262	0.04257	0.04251	0.04250

Results demonstrate that the accuracy of SHBNM decreases when R approaches to 5.0. And when R=4.999, SHBNM get wrong results, and degenerate at R=4.9999. RHBNM, however, achieves very high accuracy in the whole range of values of R. Moreover, further RHBNM computation has been performed for R=5.0. It is found that results are the same as the case that R=4.9999.

5. Concluding remarks

SHBNM and RHBNM have been compared in several aspects in this paper. Both the methods have advantages and disadvantages. RHBNM is suitable for solving structures of simple and regular shapes. For such kind of structures, RHBNM can achieve very high accuracy even with a small number of nodes. One of the main disadvantages of RHBNM is its low convergence rate and instability. The accuracy is strongly dependent on the scale factor *SF*. SHBNM, on the other hand, is stable and possesses higher convergence rate than RHBNM.

The applicability of RHBNM and SHBNM to analysis of thin structures has also been studied. Results clearly demonstrate that RHBNM can solve thin structure problems of simple and regular shapes with high accuracy, even when the thickness to length ratio of the structure is in micro scale. SHBNM, however, fails when the thickness to length ratio reaches 10^{-4}.

Combining RHBNM and SHBNM in multi-domain analysis of complicated structures which contains very thin sub-structures (nanotube based composites, for example) is a promising topic of future research work.

Acknowledgements

This work was supported by the CLUSTER of Ministry of Education, Culture, Sports, Science and Technology (Japan).

References

1. Mukherjee Y.X., Mukherjee S., The boundary node method for potential problems, Int. J. Numer. Meth. Engng., Vol. 40 (1997), pp. 797-815.
2. Belytchko T., Krongauz Y., Organ D., Fleming M., Krysl P., Meshless methods: an overview and recent developments, Computer Methods in Applied Mechanics and Engineering, Vol. 139 (1996), pp. 3-47.
3. Zhang, J.M., Yao, Z.H., Li, H., A hybrid boundary node method, Int. J. Numer. Meth. Engng., Vol. 53 (2002), pp. 751-763.
4. Zhang J.M., Yao Z.H., Meshless regular hybrid boundary node method, Computer Modeling in Engineering & Sciences, Vol. 2 (2001), pp. 307-318.
5. DeFigueredo T.G.B., Brebbia C.A., A new hybrid displacement variational formulation of BEM for elastostatics. Brebbia CA and Conner JJ (eds.), Advances in Boundary Elements, CMP 1989; 1:47-57.
6. Atluri S.N., Kim H.G., Cho J.Y., A critical assessment of the truly Meshless Local Petrov-Galerkin (MLPG), and Local Boundary Integral Equation (LBIE) methods, Computational Mechanics, Vol. 24 (1999) pp. 348-372.
7. Zhang, J.M., Tanaka, M., Matsumoto, T., Meshless analysis of potential problems in three dimensions with the hybrid boundary node method, Int. J. Numer. Meth. Engng., to appear.
8. Zhang J.M., Yao Z.H., Analysis of 2-D thin structures by the meshless regular hybrid boundary node method, Acta Mechanica Sinica, Vol. 15 (2002), pp. 36-44.